

## Electronic Supplementary Information

# Highly reversible sorption of H<sub>2</sub>S and CO<sub>2</sub> by an environmentally-friendly Mg-based MOF

*Eli Sánchez-González,<sup>a†</sup> Paulo G. M. Mileo,<sup>b†</sup> Mónica Sagastuy-Breña,<sup>a</sup> J. Raziel  
Álvarez,<sup>a</sup> Joseph Reynolds,<sup>c</sup> Aline Villarreal,<sup>d</sup> Aída Gutiérrez-Alejandre,<sup>d</sup> Jorge  
Ramírez,<sup>d</sup> Jorge Balmaseda,<sup>a</sup> Eduardo González-Zamora,<sup>e</sup> Guillaume Maurin,<sup>b,\*</sup> Simon  
Humphrey<sup>c,\*</sup> and Ilich A. Ibarra<sup>a,\*</sup>*

<sup>a</sup>Laboratorio de Fisicoquímica y Reactividad de Superficies (LaFREs), Instituto de Investigaciones en Materiales, Universidad Nacional Autónoma de México, Circuito Exterior s/n, CU, Del. Coyoacán, 04510, Ciudad de México, Mexico.

<sup>b</sup>Institut Charles Gerhardt Montpellier, UMR-5253, Université de Montpellier, CNRS, ENSCM, Place E. Bataillon, 34095 Montpellier cedex 05, France.

<sup>c</sup>Department of Chemistry, The University of Texas at Austin, Welch Hall 2.204, 105 East 24<sup>th</sup> St., Stop A5300, Austin, Texas 78712-1224, United States.

<sup>d</sup>UNICAT, Departamento de Ingeniería Química, Facultad de Química, Universidad Nacional Autónoma de México (UNAM), Coyoacán, Ciudad de México, Mexico.

<sup>e</sup>Departamento de Química, Universidad Autónoma Metropolitana-Iztapalapa, San Rafael Atlixco 186, Col. Vicentina, Iztapalapa, C. P. 09340, Ciudad de México, Mexico.

<sup>†</sup>These authors contributed equally to this work.

## 1. Experimental

**Thermogravimetric Analysis (TGA)**, were performed in a TA Instruments Thermobalance, Q500 HR under N<sub>2</sub> atmosphere using the Hi-Res mode with a maximum rate of 5 K min<sup>-1</sup> (sensitivity 1, res. 5), from room temperature to 1073 K.

**Powder X-ray Diffraction Patterns (PXRD)**, were collected on a Rigaku Diffractometer, Ultima IV with a Cu-K $\alpha$ 1 radiation ( $\lambda = 1.5406 \text{ \AA}$ ) using a nickel filter. Patterns were recorded in the 5-50° 2 $\theta$  range with a step scan of 0.02° and a scan rate of 0.08° min<sup>-1</sup>.

**Scanning Electron Microscopy images (SEM)**, were recorded using a JEOL Benchtop Scanning Electron Microscope, Neoscope JCM-6000 using secondary electrons at 15 kV current in high vacuum.

**H<sub>2</sub>S Breakthrough experiments**, the H<sub>2</sub>S determination was made using a HP 5890 GC, by continuous injections of the system exhaust, of each injection we obtained a chromatogram. From the corresponding chromatogram we integrate the H<sub>2</sub>S signal to obtain the abundance. Knowing the H<sub>2</sub>S concentration from the feed, we can calculate the H<sub>2</sub>S concentration in each one of the injections, as the saturation concentration is the original feed concentration. From this data we can obtain the corresponding breakthrough plots, C/C<sub>f</sub> vs time. In this system it is necessary carry out a Blank, because the system can adsorb H<sub>2</sub>S by itself.

## 2. Thermogravimetric Analysis

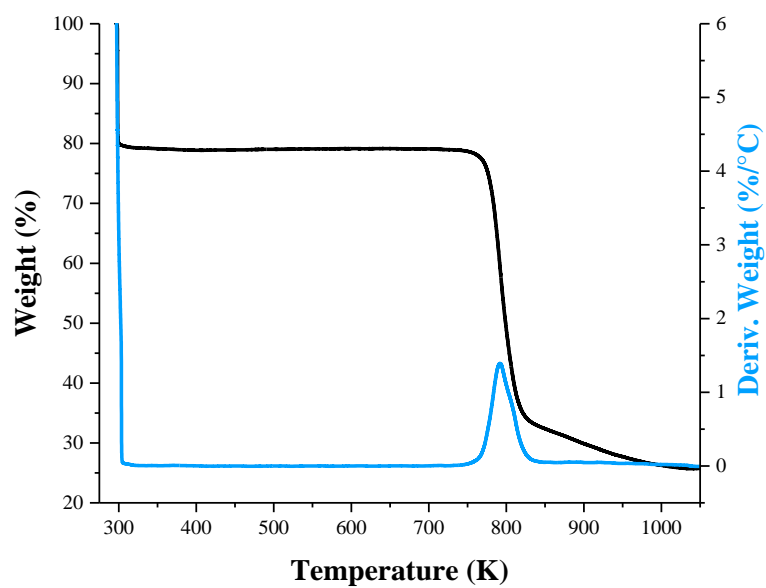


Fig. S1. TGA trace of Mg-CUK-1 as synthesized.

## 3. Powder X-ray Diffraction Patterns

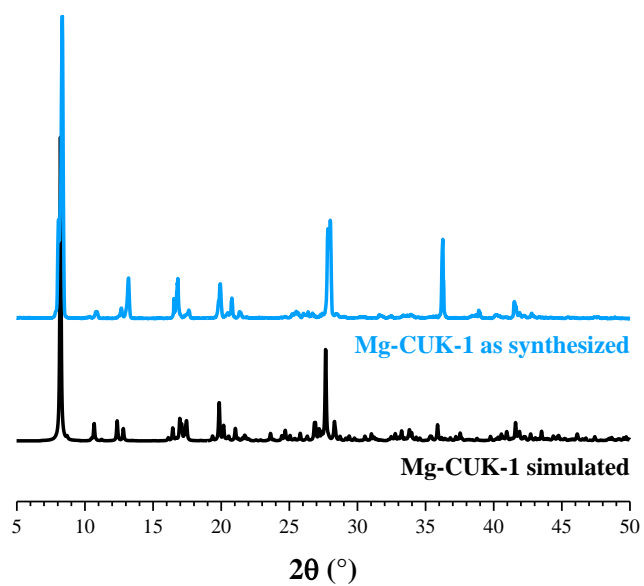


Fig. S2. PXRD patterns of Mg-CUK-1 simulated (black) and as synthesized (blue).

#### 4. BET area

Since Mg-CUK-1 shows no adsorption of N<sub>2</sub> at 77 K, CO<sub>2</sub> adsorption isotherms at 196 K were measured to evaluate the surface area of the material as reported before.<sup>1</sup> The Brunauer–Emmett–Teller (BET) analysis was used to estimate the textural properties.<sup>2</sup> Fig. S3A features the CO<sub>2</sub> adsorption isotherm at 196 K, it shows a type II isotherm shape corresponding to a microporous material.

Before the surface area estimation, a  $n(1-P/P_0)$  vs  $P/P_0$  plot (Fig. S3B) was used to assess the data range where the BET theory is valid.<sup>2,3</sup> In this equation ‘n’ corresponds to the adsorbed amount (mol g<sup>-1</sup>) and ‘ $P/P_0$ ’ to the partial pressure, the latter estimated with  $P_0 = 1.035$  bar.<sup>4</sup> The data range was limited to only where  $n(1-P/P_0)$  continuously increased with  $P/P_0$ . Thus, it was taken only data below the maximum point ( $n(1-P/P_0)$ ) for this calculation (see Fig. S3B,  $0.005 < P/P_0 < 0.15$ ). From the BET equation (Eq. S1) the monolayer capacity ‘ $n_m$ ’ (mol g<sup>-1</sup>) and ‘C’ parameter can be estimated by using the slope and intercept of the linear fitted data using Eqs. S1 & S2 (Fig. S3C). The value of C was found to 163, i.e. a positive value which is consistent with the validity of the BET method.

$$\frac{P/P_0}{n(1-P/P_0)} = \frac{1}{n_m C} + \frac{C-1}{n_m C} (P/P_0) \quad \text{Eq. S1}$$

$$n_m = \frac{1}{\text{slope} + \text{intercept}} \quad \text{Eq. S2}$$

$$C = 1 + \text{slope} + \text{intercept} \quad \text{Eq. S3}$$

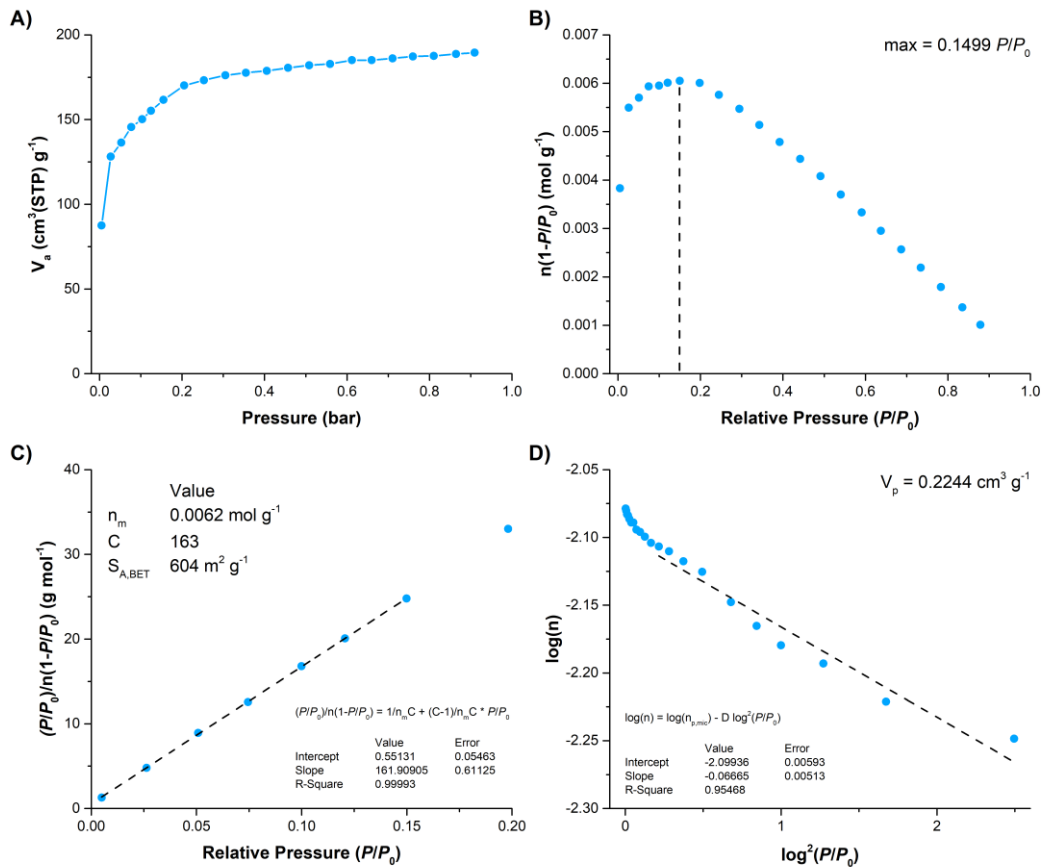


**Fig. S3.** Mg-CUK-1 as synthesized A) CO<sub>2</sub> adsorption isotherm at 196 K; B)  $n(1-P/P_0)$  vs  $P/P_0$  plot, only data below  $P/P_0 = 0.1499$  was used in the BET method; C) BET plot with linear fitting to estimate the surface area; D) DR plot with linear fitting to estimate the pore volume.

The surface area was then estimated by Eq. S4, where ' $n_m$ ' is the monolayer capacity ( $\text{mol g}^{-1}$ ), ' $L$ ' is the Avogadro's number ( $6.02214179 \cdot 10^{23} \text{ mol}^{-1}$ ), and ' $\sigma$ ' is the cross-sectional area of the adsorbent ( $\sigma_{CO_2} = 0.163 \text{ nm}^2$ ). Using the monolayer capacity  $n_m = 0.0062 \text{ mol g}^{-1}$ , the estimated surface area for Mg-CUK-1 is  $S_{A,BET} = 604 \text{ m}^2 \text{ g}^{-1}$  (Fig. S3C).

$$S_{A,BET} = n_m \cdot L \cdot \sigma \quad \text{Eq. S4}$$

Additionally, the pore volume was estimated using a Dubinin–Radushkevich (DR) plot (Fig. S3D) following Eq. S5.<sup>2</sup> Where  $D$  is an empirical constant and from the intercept the specific micropore capacity ' $n_{p,mic}$ ' ( $\text{mol g}^{-1}$ ) is obtained. This micropore capacity is used to estimate the micropore volume ' $V_{p,mic}$ ' ( $\text{cm}^3 \text{ g}^{-1}$ ) by using Eq. S6, where ' $M$ ' and ' $\rho$ ' are the molar mass and density of the adsorbent respectively ( $M_{CO_2} = 44.01 \text{ g mol}^{-1}$  and  $\rho_{CO_2} = 1.56 \text{ g cm}^{-3}$ ). From the linear fitting of the DR plot in Fig. S3D  $n_{p,mic} = 0.00795 \text{ mol g}^{-1}$  was obtained and the pore volume of Mg-CUK-1 was estimated  $V_p = 0.2244 \text{ cm}^3 \text{ g}^{-1}$ .

$$\log(n) = \log(n_{p,mic}) + D \log^2(P/P_0) \quad \text{Eq. S5}$$

$$V_{p,mic} = n_{p,mic} \cdot \frac{M}{\rho} \quad \text{Eq. S6}$$

BET area analysis was used to assess the retention of the Mg-CUK-1 adsorption properties after exposure to  $\text{H}_2\text{O}$ . A Mg-CUK-1 sample was activated at 373 K for 1 hour under flowing  $\text{N}_2$  in a DVS Advantage 1 instrument from Surface Measurement System. In the same instrument, the Mg-CUK-1 sample was maintained for 2 hours with 95% of Relative Humidity at 303 K, then the RH was set to zero before the sample removal. After the water exposure, the Mg-CUK-1 sample was taken to a Belsorp HP analyser to perform a  $\text{CO}_2$  adsorption isotherm, prior measurement the sample was activated again at 373 K for 1 hour under high vacuum.

The CO<sub>2</sub> adsorption isotherm collected at 196 K for Mg-CUK-1 that initially underwent a 8 water adsorption cycle, did not show a significant difference from the as-synthesised sample (Fig. S4A). The same BET analysis was applied to this data, then the BET area (Fig. S4C) and pore volume (Fig. S4D) were estimated,  $S_{A,BET} = 586 \text{ m}^2 \text{ g}^{-1}$  and  $V_p = 0.2257 \text{ cm}^3 \text{ g}^{-1}$ , these values did not differ much from the as-synthesised sample (only 3% loss of surface area).

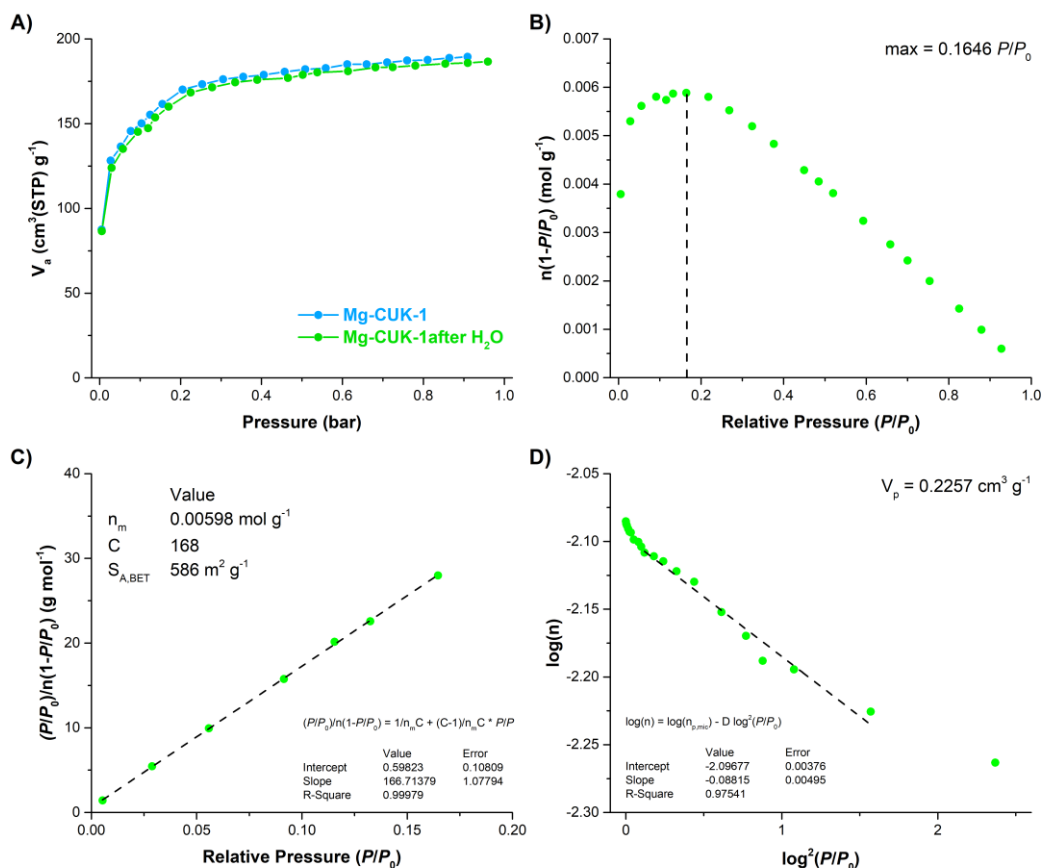


**Fig. S4.** Mg-CUK-1 after 8 cycles of H<sub>2</sub>O adsorption A) CO<sub>2</sub> adsorption isotherm compared with the as-synthesised sample at 196 K; B)  $n(1-P/P_0)$  vs  $P/P_0$  plot, only data below  $P/P_0 = 0.1646$  was used in the BET method; C) BET plot with linear fitting to estimate the surface area; D) DR plot with linear fitting to estimate the pore volume.

The CO<sub>2</sub> adsorption isotherm at 196 K for Mg-CUK-1 after H<sub>2</sub>S adsorption, did not show a considerable difference from the as-synthesised sample (Fig. S5A). The same BET analysis was applied to these data, then the BET area (Fig. S5C) and pore volume (Fig. S5D) were estimated,  $S_{A,BET} = 597 \text{ m}^2 \text{ g}^{-1}$  and  $V_p = 0.2249 \text{ cm}^3 \text{ g}^{-1}$ . Essentially, these values did not differ from the as-synthesised sample (1% loss of surface area).

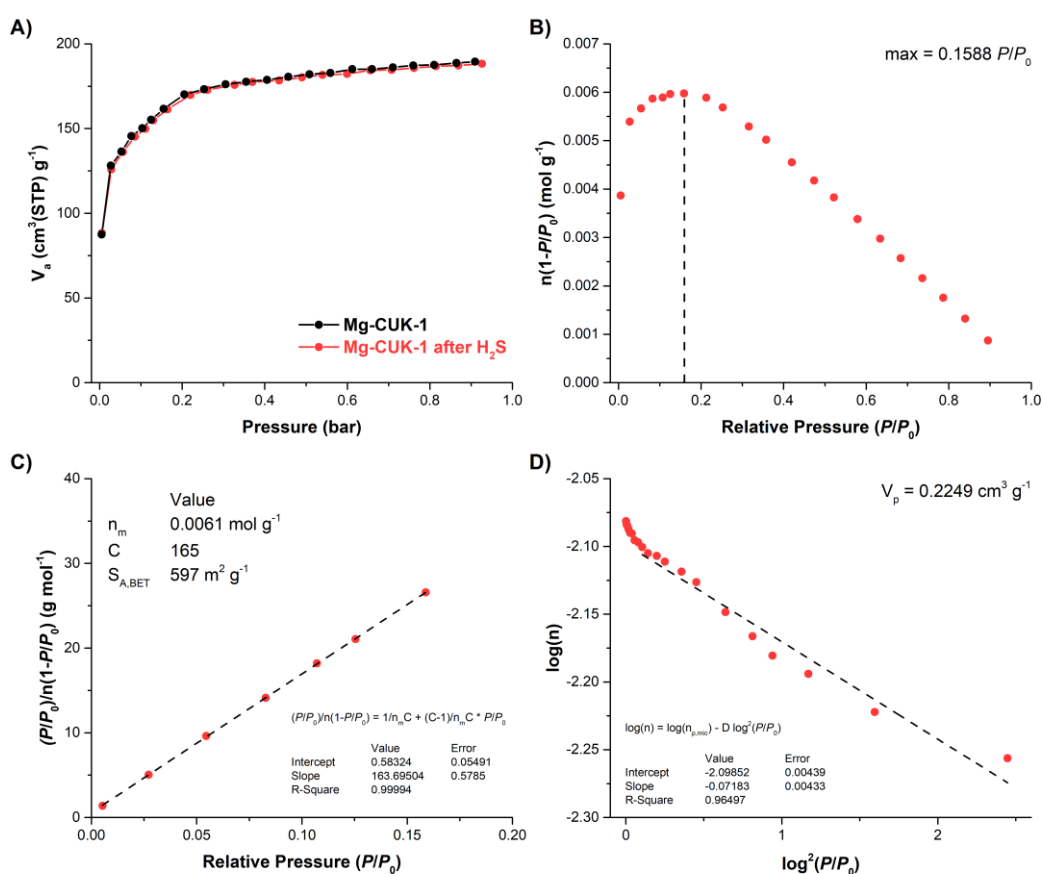


**Fig. S5.** Mg-CUK-1 after H<sub>2</sub>S adsorption A) CO<sub>2</sub> adsorption isotherm compared with the as-synthesised sample at 196 K; B)  $n(1-P/P_0)$  vs  $P/P_0$  plot, only data below  $P/P_0 = 0.1588$  was used in the BET method; C) BET plot with linear fitting to estimate the surface area; D) DR plot with linear fitting to estimate the pore volume.

## 5. Atomic partial charges

Atomic partial charges were estimated from the periodic DFT optimized anhydrous Mg-CUK-1 framework with the Repeating Electrostatic Potential Extracted Atomic (REPEAT) fitting approach. In Figure S6 and Table S1 the atom types and their consecutive atomic partial charges are respectively provided.

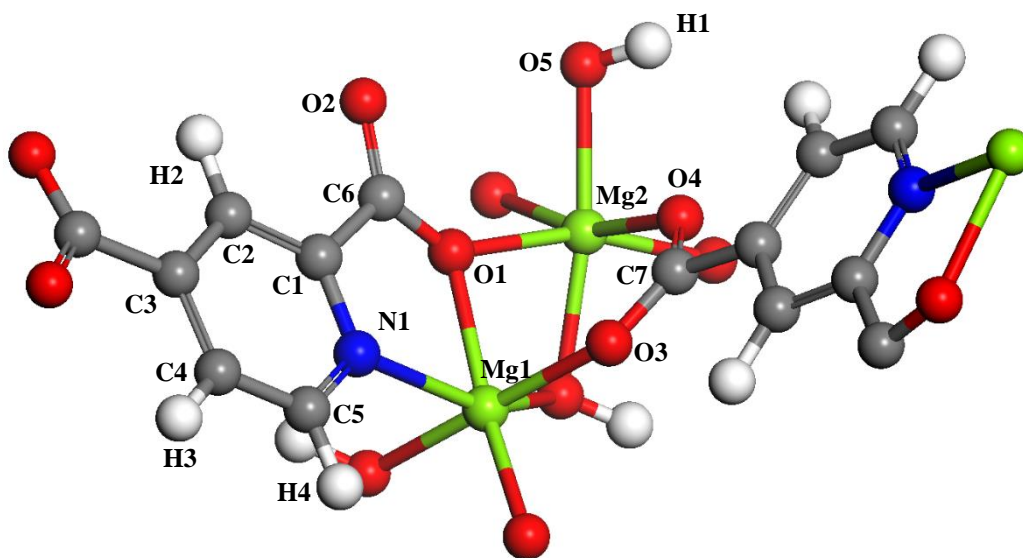


**Fig. S6.** Identification of the atom types in the Mg-CUK-1.

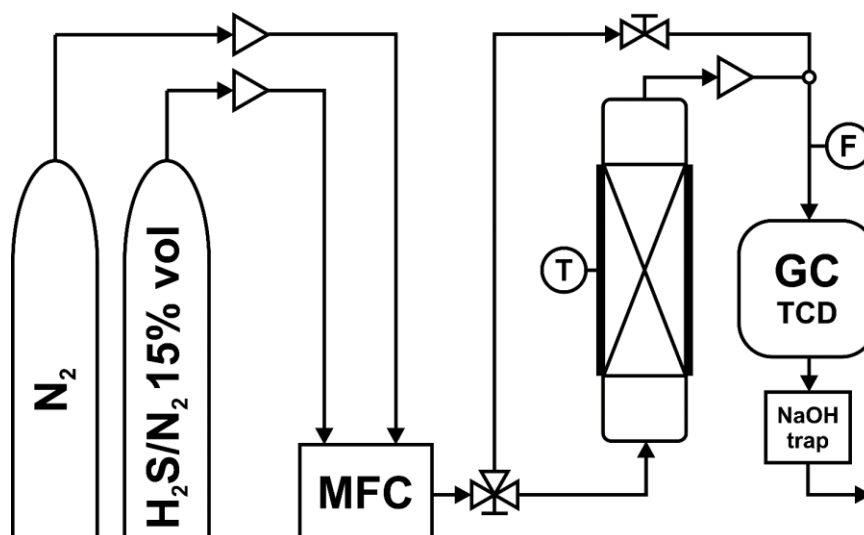
**Table S1.** Atomic partial charges assigned to each one of the atom types in the Mg-CUK-1.

<b>Atom type</b>	<b>q (e)</b>
C1	0.4806
C2	-0.4388
C3	0.2215
C4	-0.2949
C5	0.2230
C6	0.3581
C7	0.6515
O1	-0.5425
O2	-0.5271
O3	-0.6784
O4	-0.6801
O5	-1.1055
H1	0.3984
H2	0.2017
H3	0.1537
H4	0.0408
N1	-0.4720
Mg1	1.2971
Mg2	1.4260

## 6. Hydrogen sulfide adsorption

Dynamic breakthrough experiments were carried out in a home-made system (Scheme S1). The adsorption column was made from quartz glass with an internal diameter of 7 mm, with a porous glass bed to hold the sample. The adsorption column was covered with a temperature-controlled heating jacket. The column downstream was monitored with a gas chromatograph (HP-5890) equipped with a HP-PLOT 1 column and a thermal conductivity detector (TCD). The GC is equipped with an automatic injection valve which samples every 30 s.

In a typical experiment, 50 mg of Mg-CUK-1 sample were activated *in situ* at 373 K for 1 hour with a constant flow of dry N<sub>2</sub> and then slowly cooled to 303 K. Then the H<sub>2</sub>S desired concentration was adjusted with a mass flow controller fed with two lines: dry N<sub>2</sub> and H<sub>2</sub>S/N<sub>2</sub> 15 %vol (Scheme S1), by adjusting the percentage of each feed, with a maximum H<sub>2</sub>S concentration of 15 %vol. The breakthrough experiments were carried out at 303 K and the downstream flow was analysed with a GC every 30 s, the complete breakthrough of H<sub>2</sub>S was indicated by the downstream gas concentration reaching the initial feed.



**Scheme S1.** Representation of breakthrough system. The H<sub>2</sub>S/N<sub>2</sub> mixture passed through a mass flow controller (MFC) which feeds the adsorption column, and a gas chromatograph with a thermal conductivity detector (GC TCD) was used to measure the H<sub>2</sub>S downstream.

The H<sub>2</sub>S adsorption capacity of Mg-CUK-1 was calculated using Eq. S7, where ' $V_{H_2S}$ ' represents the H<sub>2</sub>S volumetric capacity (cm<sup>3</sup> g<sup>-1</sup>), ' $m$ ' the adsorbent mass (g), ' $F$ ' the input flow rate (cm<sup>3</sup> min<sup>-1</sup>), ' $C_f$ ' and ' $C_t$ ' the influent and downstream H<sub>2</sub>S concentrations respectively (% vol), and ' $t$ ' the time (min).<sup>5</sup>

$$V_{H_2S} = \frac{F}{C_f \cdot m} \cdot \int_0^t (C_f - C_t) dt \quad \text{Eq. S7}$$

As mentioned before, the adsorption column has a porous glass bed thus, a blank run before each experiment was measured to eliminate the adsorption contribution of the column. In Fig. S7 the blue circles represent the adsorption of the column, and the black circles represent the

Mg-CUK-1 adsorption. Then the Mg-CUK-1 corrected volumetric capacity ' $V_{H_2S,corr}$ ' was estimated using Eq. S8.

$$V_{H_2S,corr} = V_{H_2S,blank} - V_{H_2S,sample} \quad \text{Eq. S8}$$

The H<sub>2</sub>S adsorption capacity is often reported as ' $q_{H_2S}$ ' (mol g<sup>-1</sup>), this value was roughly estimated with the volumetric adsorption capacity ' $V_{H_2S,corr}$ ' (cm<sup>3</sup> g<sup>-1</sup>) and the ideal gas law Eq. S9. Where ' $p$ ' is the system pressure (77.3 kPa), ' $T$ ' the measurement temperature (303 K), and ' $R$ ' the ideal gas constant (8314.4598 cm<sup>3</sup> kPa K<sup>-1</sup> mol<sup>-1</sup>).

$$q_{H_2S} = \frac{V_{H_2S,corr} \cdot p}{R \cdot T} \quad \text{Eq. S9}$$

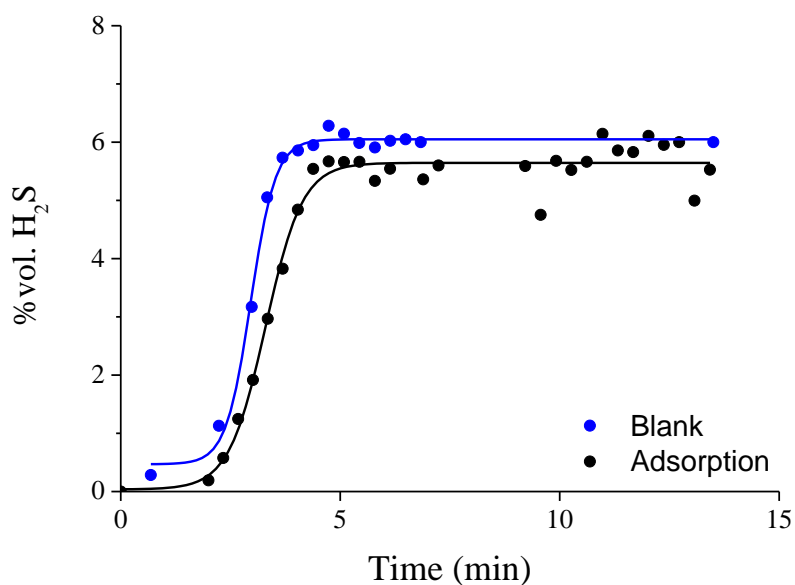


**Fig. S7.** H<sub>2</sub>S adsorption breakthrough curves of Mg-CUK-1 at 303 K using a 6 %vol. H<sub>2</sub>S/N<sub>2</sub> feed concentration. The circles represent the experimental data for the sample (black) and the empty cell (blue), solid lines represent the sigmoidal fit. Flow rate was adjusted to 30 cm<sup>3</sup> min<sup>-1</sup>.

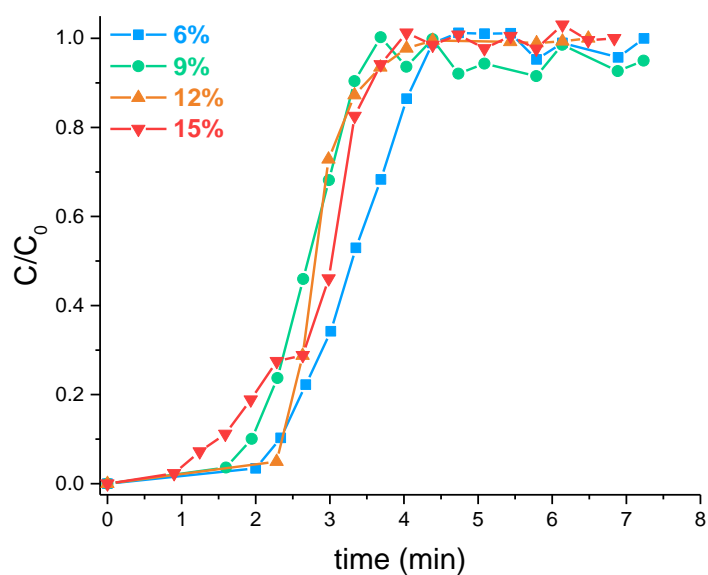


**Fig. S8.** H<sub>2</sub>S adsorption breakthrough curves of Mg-CUK-1 at 303 K using different %vol. H<sub>2</sub>S/N<sub>2</sub> feed concentration. Flow rate was adjusted to 30 cm<sup>3</sup> min<sup>-1</sup>.

The breakthrough system was tested with other reported MOF materials (Fig. S9): MOF-74(Zn), HKUST-1 and MIL-101(Cr).<sup>6</sup> 50 mg of each sample were activated *in situ* at 453 K for 1 hour with a constant flow of dry N<sub>2</sub> and then slowly cooled to 303 K. Then the H<sub>2</sub>S desired concentration was adjusted 6 %vol. Adsorption capacity at 6 %vol of H<sub>2</sub>S concentration for the reported materials are correspondent with the reported values (Table S2).

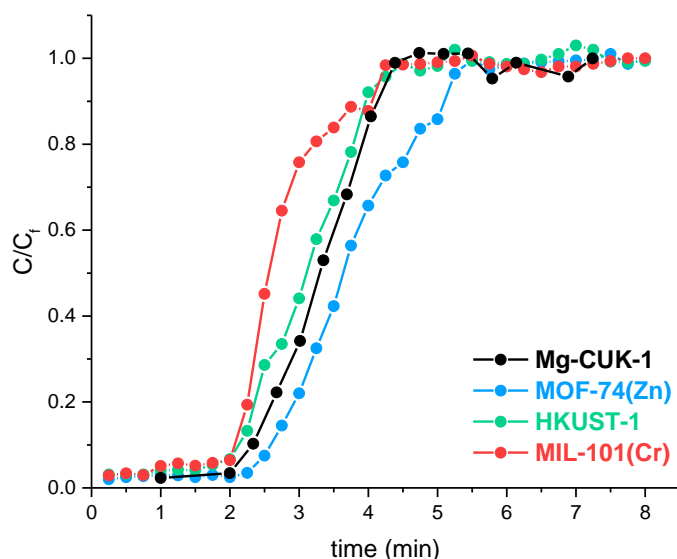


**Fig. S9.** H<sub>2</sub>S adsorption breakthrough curves at 303 K for Mg-CUK-1, MOF-74(Zn), HKUST-1 and MIL-101(Cr). Measurements using 6 %vol. H<sub>2</sub>S/N<sub>2</sub> feed concentration and a 30 cm<sup>3</sup> min<sup>-1</sup> flow rate.

**Table S2.** H<sub>2</sub>S adsorption capacity for Mg-CUK-1 and related materials. Breakthrough measurements using 6 %vol. H<sub>2</sub>S/N<sub>2</sub> feed concentration and a 30 cm<sup>3</sup> min<sup>-1</sup> flow rate.

Material	H <sub>2</sub> S uptake (mmol g <sup>-1</sup> )	
	This work	Reported <sup>b</sup>
Mg-CUK-1	1.41	-
MOF-74(Zn)	1.72	1.64
HKUST-1	1.04	1.1
MIL-101(Cr)	0.52	0.4

In order to investigate the H<sub>2</sub>S regeneration-capacity and the structure stability of Mg-CUK-1 (Fig. S10), cycling H<sub>2</sub>S experiments at 15 %vol H<sub>2</sub>S were then performed on the same Mg-CUK-1 sample. After the H<sub>2</sub>S adsorption a re-activation process was carried out, then a PXRD pattern of the sample was measured to assess the retention of crystallinity (Fig. S11). After the PXRD a CO<sub>2</sub> adsorption isotherm was measured at 196 K to corroborate the retention of the surface area 592.4±7.6 m<sup>2</sup> g<sup>-1</sup> (Fig. S12). Finally, an additional CO<sub>2</sub> adsorption isotherm at 303

K was measured up to 6 bar as a to prove the retention of the adsorption properties of Mg-CUK-1, total CO<sub>2</sub> uptake of 5.93±0.12 mmol g<sup>-1</sup>. The overall adsorption properties remained after five H<sub>2</sub>S adsorption cycles (Table S3).

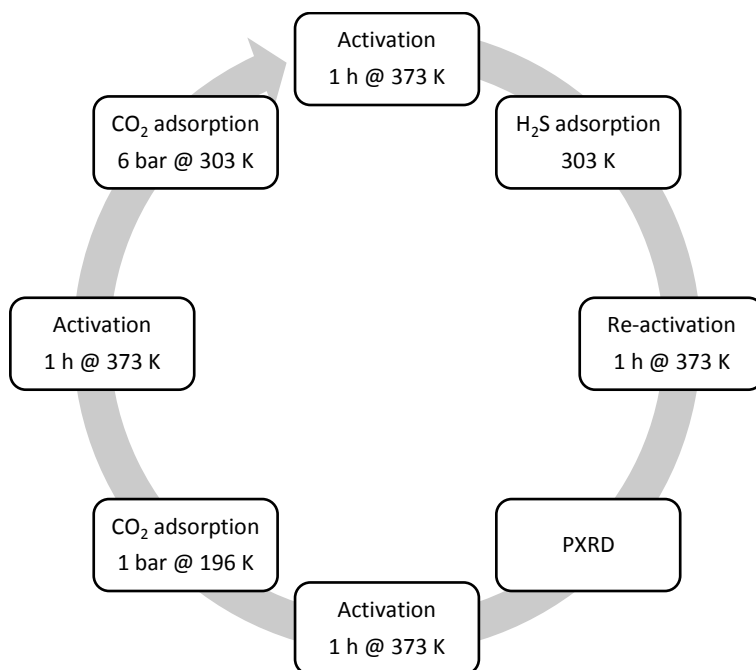


**Fig. S10.** Mg-CUK-1 activation-H<sub>2</sub>S adsorption cycle procedure, PXR D and CO<sub>2</sub> adsorption isotherms after each cycle.

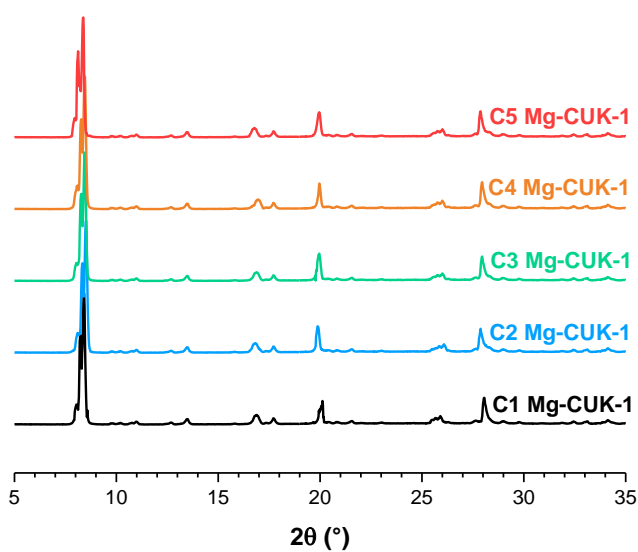


**Fig. S11.** PXR D patterns of Mg-CUK-1, after each H<sub>2</sub>S adsorption cycle.

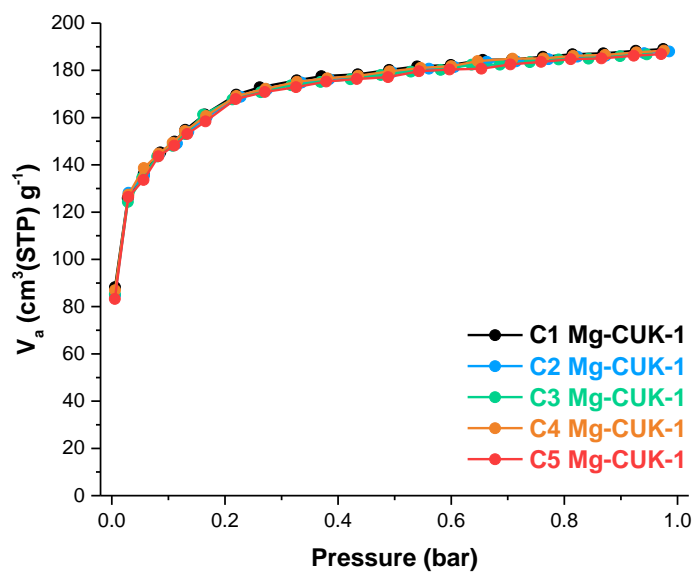


**Fig. S12.** CO<sub>2</sub> adsorption isotherms of Mg-CUK-1 at 196 K, after each H<sub>2</sub>S adsorption cycle.

**Table S3.** Adsorption properties of Mg-CUK-1 after H<sub>2</sub>S adsorption cycles.

Cycle	H <sub>2</sub> S uptake (mmol g <sup>-1</sup> )	S <sub>A,BET</sub> (m <sub>2</sub> g <sup>-1</sup> )	CO <sub>2</sub> uptake (mmol g <sup>-1</sup> )
1	3.45	597	5.87
2	3.12	590	5.85
3	3.02	601	6.09
4	3.33	593	6.02
5	3.09	581	5.82

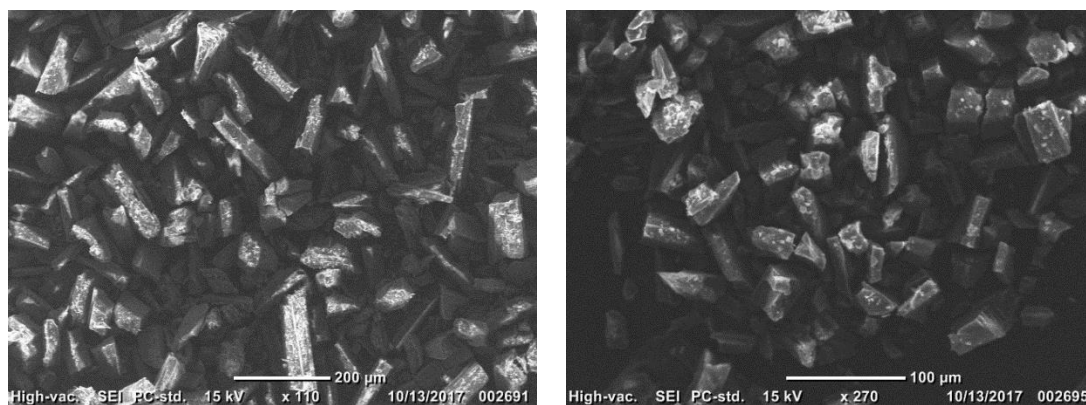


**Fig. S13.** Mg-CUK-1 SEM images before (left) and after H<sub>2</sub>S adsorption (right).

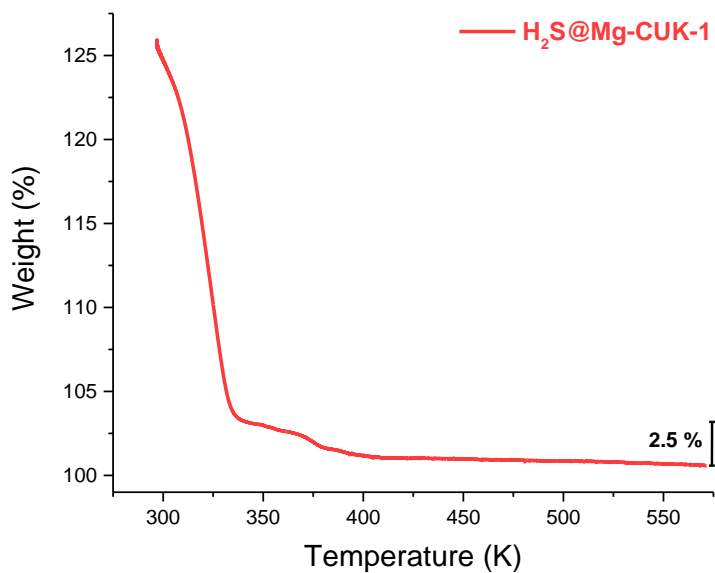


**Fig. S14.** TGA trace of the H<sub>2</sub>S partially saturated Mg-CUK-1 sample correcting the 100 wt% to “empty” weight, marking the weight loss corresponding to the captured H<sub>2</sub>S.

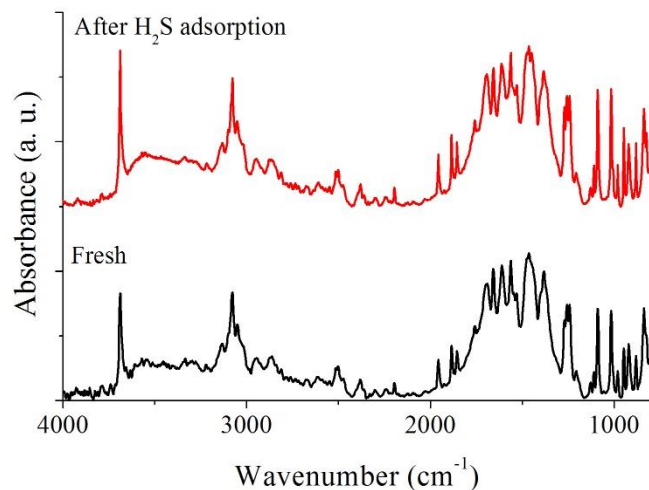


**Fig. S15.** DRIFT spectra of Mg-CUK-1 evacuated at  $6.43 \times 10^{-3}$  Torr at room temperature, before (black) and after H<sub>2</sub>S adsorption (red).

## 7. Flexibility of Mg-CUK-1 upon H<sub>2</sub>S adsorption

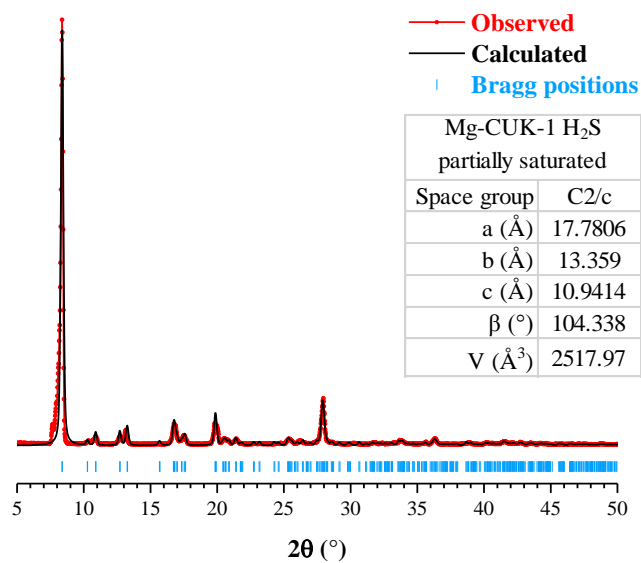


**Fig. S16.** Mg-CUK-1 Le Bail refinement of the H<sub>2</sub>S partially saturated sample.

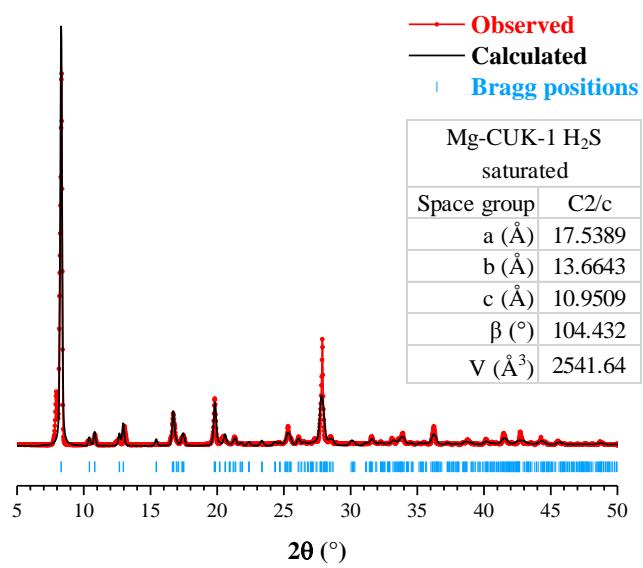
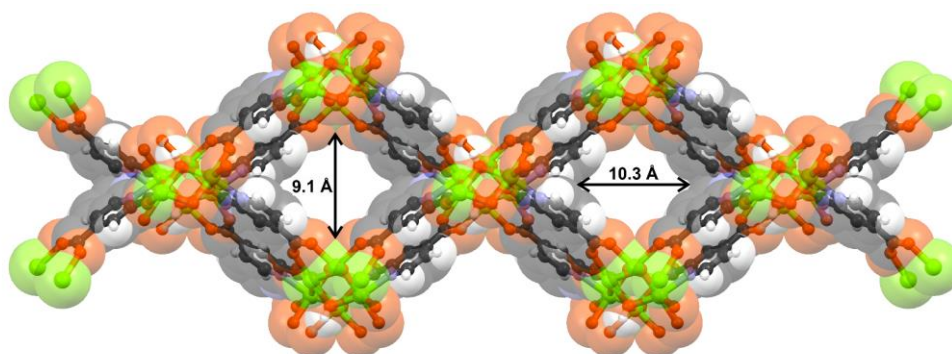
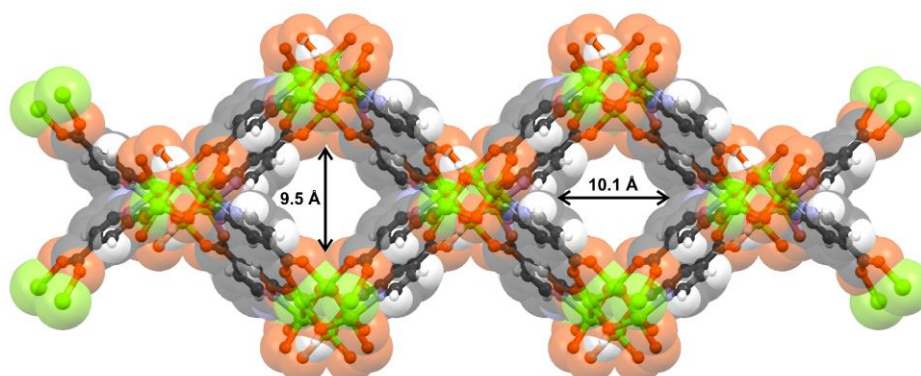


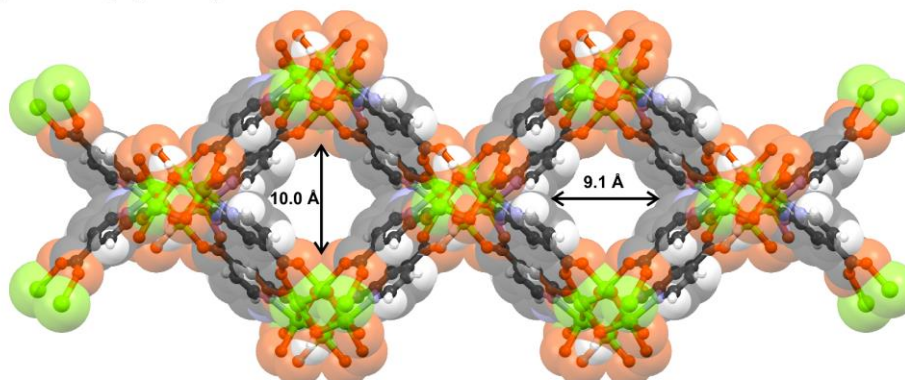
**Fig. S17.** Mg-CUK-1 Le Bail refinement of the H<sub>2</sub>S saturated sample.



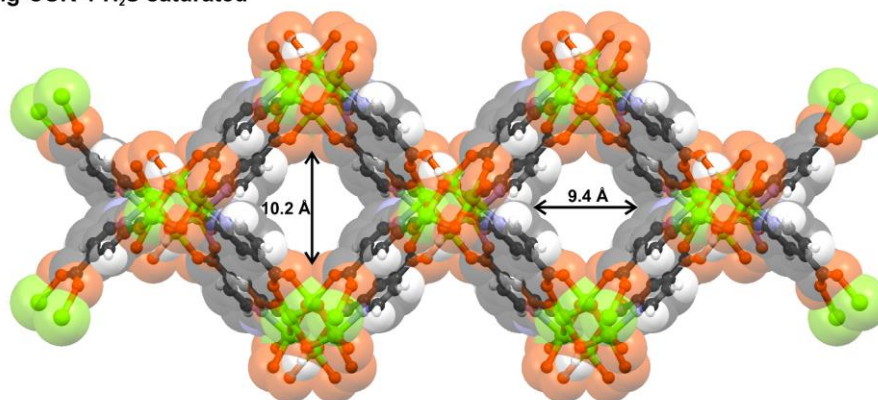
**Mg-CUK-1 anhydrous**



**Mg-CUK-1 H<sub>2</sub>S partially saturated**



**Mg-CUK-1 H<sub>2</sub>S saturated**



**Mg-CUK-1 H<sub>2</sub>O saturated**

**Fig. S18.** Mg-CUK-1 channel dimensions at different guest conditions.

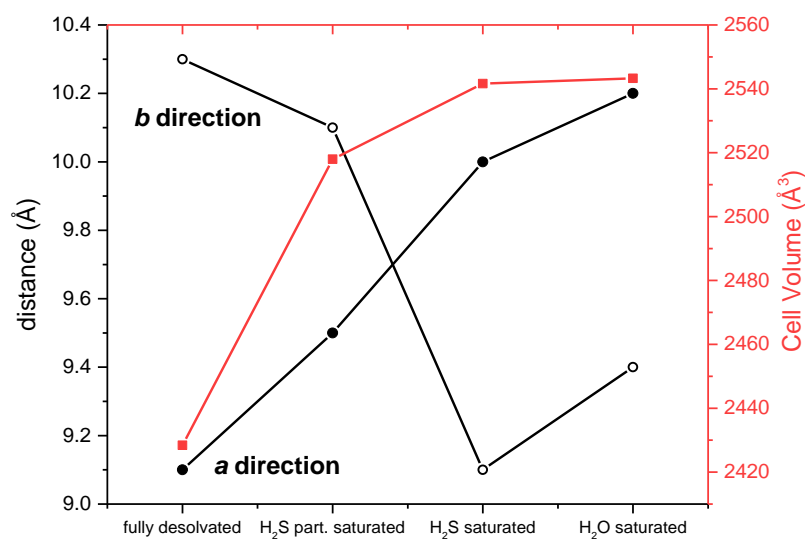


**Fig. S19.** Mg-CUK-1 change in the dimensions of the channel (*a* and *b* direction) and Cell volume.

## References

1. B. Saccoccia, N. W. Waggoner, K. Cho, S. Lee, D. Hong, M. Alisha, V. M. Lynch, J. Chang and S. M. Humphrey, *Angew. Chem. Int. Ed.*, 2015, **54**, 5394.
2. F. Rouquerol, J. Rouquerol, K.S.W. Sing, P. Llewellyn and G. Maurin, *Adsorption by Powders and Porous Solids: Principles, Methodology and Applications*, Academic Press, Oxford, 2<sup>nd</sup> edn, 2014, pp. 237–251, 303–309.
3. K. S. Walton and R. Q. Snurr, *J. Am. Chem. Soc.*, 2007, **129**, 8552.
4. E. Fernández-Fassnacht and F. Del Río, *J. Chem. Thermodynamics*, 1984, **16**, 469.
5. P. Nugent, Y. Belmabkhout, S. D. Burd, A. J. Cairns, R. Luebke, K. Forrest, T. Pham, S. Ma, B. Space, L. Wojtas, M. Eddaoudi, and M. J. Zaworotko, *Nature*, 2013, **495**, 80.
6. J. Liu, Y. Wei, P. Li, Y. Zhao and R. Zou, *J. Phys. Chem. C*, 2017, **121**, 13249.